Sensors and Materials, Vol. 26, No. 1 (2014) 19–30
MYU Tokyo

S & M 0966

Zirconia Ceramics Applied in a Pressure-Sensitive Device Fabricated Using HTCC Technology

Qiu Lin Tan[1,2,3], Li Qin[1,2,*], Hao Kang[1,2,**], Ji Jun Xiong[1,2,***], Wen Dong Zhang[1,2], Tao Luo[1,2], Chen Li[1,2], Li Qiong Ding[1,2], Xian Sheng Zhang[1,2] and Ming Liang Yang[1,2]

[1]Key Laboratory of Instrumentation Science & Dynamic Measurement, Ministry of Education, North University of China, Tai Yuan 030051, China
[2]Science and Technology on Electronic Test & Measurement Laboratory, North University of China, Tai Yuan 030051, China
[3]National Key Laboratory of Fundamental Science of Micro/Nano-Device and System Technology, Chongqing University, Chong Qing 400044, China

(Received June 16, 2013; accepted September 9, 2013)

Key words: zirconia ceramic, high-temperature cofired ceramics (HTCC), capacitive pressure sensor, wireless passive sensor, LC circuit, mutual inductance coupling

A wireless passive high-temperature cofired ceramic (HTCC) pressure sensor fabricated from partially stabilized zirconia (PSZ) ceramic is proposed. This sensor can be used in high-temperature environments (in excess of 1000 °C in some cases) owing to its high mechanical strength at high thermal stress, and pressure data can be transmitted through mutual inductance coupling. Experimental systems are designed to obtain the necessary frequency-pressure and frequency-temperature characteristics. The experimental results between room temperature and 800 °C (and then at 800 °C for 30 min) indicate that the sensor has improved stability at 800 °C and the sensor also shows a high sensitivity at room temperature.

1. Introduction

High-temperature pressure sensors are widely used in the latest generation of weapon and equipment systems, as they can be used to measure pressure at the surfaces of jet engines, rockets, missiles, satellites, and similar devices.[(1)] Such sensors have great significance in enabling safe operation and precise system performance control through their ability to deliver real-time pressure data accurately in high-thermal-stress environments.[(2)]

*Corresponding author: e-mail: qinli@nuc.edu.cn
**Corresponding author: e-mail: kanghao_0217@sina.com
***Corresponding author: e-mail: tanqiulin@nuc.edu.cn

Piezoresistive pressure sensors are widely used in high-temperature applications, and they have many advantages in terms of small size, fast response, and a broad range of frequency responses. However, the reverse-bias operation of a Si PN junction becomes invalid at temperatures above 150 °C owing to the excitation of thermal eigenstates, causing electrical isolation to cease. Using silicon-on-insulator (SOI) materials can increase the temperature that the reverse-biased PN junction can withstand, but the sensor will still become invalid when the silicon material loses elasticity at 500 °C. Low-temperature cofired ceramic (LTCC) materials, which were introduced commercially in the early 1980s, immediately presented designers with a unique option for the manufacture of a high density of interconnect circuits.[3] Georgia Polytechnic University has developed a wireless high-temperature pressure sensor based on LTCC materials, although the structure has only been tested to 450 °C owing to test condition limitations.[4–7]

High-temperature cofired ceramic (HTCC) materials have been shown to have strong advantages for pressure measurement at temperatures above 1000 °C such as in the interior of an engine combustion chamber. Based on a detailed analysis of the defects of traditional pressure sensors used in high-temperature environments, a high-temperature HTCC-based sensor is proposed in this paper. A high-temperature elastomer material is used to solve the problem of material elasticity degeneration in high-temperature environments. Furthermore, a method of noncontact passive signal transmission measurement is used to allow the detection circuit to function in the presence of heat wire transfer. Based on its confirmed characteristics, the proposed sensor can be used to meet the testing requirements for systems ranging from hypersonic aircraft to advanced weapons engines.

2. Zirconia Ceramic and Its Molding Process

Printed film temperature sensors on fired ceramics have been used for many years and are often used for testing at several hundred degrees centigrade. As next-generation high-temperature pressure sensors need to operate at much higher temperatures (in excess of 1200 °C in some cases), there is a corresponding need to replace the printed film with HTCC materials. This is particularly true in the case of automotive sensors, for which ceramic diaphragms with great flexural strength are required.

The high-temperature HTCC-based pressure sensor presented in this paper is based on partially stabilized zirconia (PSZ) materials. PSZ is useful in the fabrication of high-temperature pressure-sensitive devices owing to its very high fracture toughness over a wide temperature range (<1850 °C) and high mechanical strength at high temperatures (<2500 °C). Zirconia has three different crystalline forms, and its stability varies with temperature as it changes between these phases. From room temperature to 1700 °C, zirconia is in the monoclinic crystal phase, then it is in the tetragonal crystal phase up to 2370 °C, and finally, it is in the cubic crystal phase from 2370 to 2680 °C. Tetragonal crystal structure and monoclinic crystal structure can be seen in Fig. 1. The change from the monoclinic to the tetragonal phase is a reversible transformation, although, in general, the crystalline phase change from cooling causes the volume to swell and the material to crack. Therefore, it is often useful to add a certain amount of stabilizer to eliminate the volume expansion brought about by crystal transformation.[8]

Partially stabilized zirconia can be obtained by adding CaO, MgO, or Y_2O_3 to pure zirconia. For example, yttrium PSZ is formed by adding 2–3 mol of Y_2O_3 and has enhanced mechanical toughness (i.e., a fracture strength greater than 1000 MPa and a fracture toughness greater than 10 MPa·m$^{1/2}$) as well as suppressed crack generation. As shown in Fig. 2, the compressive stress generated at a crack tip by a phase-change-induced volume increase can help to prevent the expansion of the crack in theory. This reinforcement mechanism, called stress-induced phase transformation toughening, makes zirconia more resilient than other ceramic materials.[9] The mechanical strength of toughened zirconia is slightly dependent on temperature, with the average strength changing from 368 MPa at room temperature to 280 MPa at 900 °C and then to 225 MPa at 1000 °C. Such features can compensate for the inherent brittleness of the high-temperature-resistant ceramic.

Figure 3, which is adapted from the experimental results reported in ref. 10, shows that zirconia has a greater high-temperature elasticity than alumina and that these elasticity properties are better maintained above 600 °C if the deformation is small.

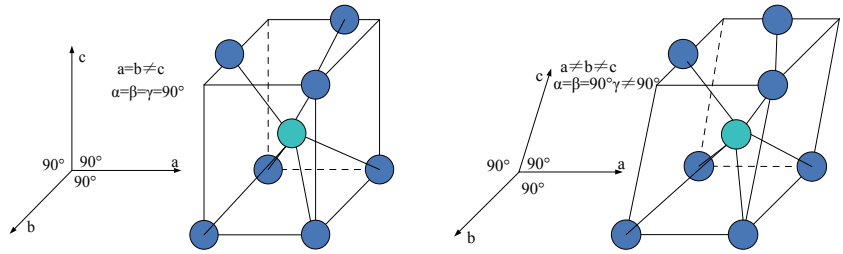

Fig. 1. (Color online) Zirconia molecular structure: (a) tetragonal crystal structure and (b) monoclinic crystal structure.

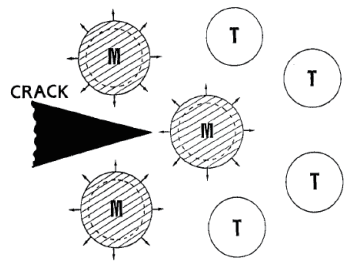

Fig. 2. PSZ phase transformation toughening diagram. The spread of cracks induces ceramic crystal changes from the metastable tetragonal to the stable monoclinic phase. Crack spread can be prevented if the size of the monoclinic crystal particles is greater than those of the tetragonal crystal.

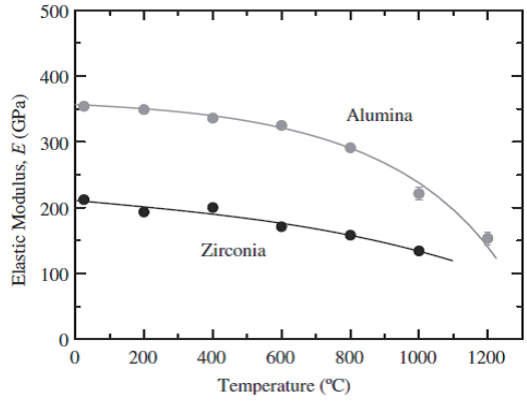

Fig. 3. Elastic modulus versus temperature.[10]

Depending on its required use, zirconia can be processed into a variety of shapes; the currently available mature zirconia molding methods are listed in Table 1.[11]

For this study, a sensor was fabricated from cast-molded zirconia green tape. Casts from a green sheet can be made into geometric solids with varying numbers of layers and thicknesses, and cast molding with a sheet multilayer stack is a preferable method of fabricating the three-dimensional structure of a fine ceramic cavity. Young's modulus E of the resulting ceramic can be obtained by measuring the maximum load P_{max}, the maximum indentation depth h_{max}, unload depth h_f, and unload curve slope S. E can be expressed using the following formula:

$$E = \frac{\pi^2}{2g\tan(\beta - \beta_r)} S, \tag{1}$$

where β is inclination of the indenter cone surface (a conical indenter with an apex angle of 120° is used in experiments), β_r is the angle of the residual indentation cone surface, and S is the unload curve slope. The cone indenter geometry factor g is $\pi\cot^2(\beta - \beta_r)$.

Indentation data for zirconia loaded at 1, 3, 5, and 7 N were obtained using the Hysitron nanoindenter, shown in Fig. 4, belonging to the Department of Materials Science and Engineering, Xi'an Jiaotong University. Based on the experimental results shown in Fig. 5, the Young's modulus from eq. (1) is 220 GPa. The characteristics of the zirconia ceramic tape are listed in Table 2.

3. Sensor Design and Fabrication

3.1 *Design*

The sensor circuit is a passive series inductance capacitance (LC) resonant circuit comprising a capacitor and a planar spiral inductor, typically with a 1:1 ratio for the

Table 1
Zirconia ceramic molding methods.

Molding method	Molding materials	Forming DOF	Uniformity	Efficiency	Costs
Mould pressing	Powder	2.5	Bad	Medium	Low
Isostatic pressing	Powder	2.5	Medium	Medium	Medium
Slip casting	Suspension	2.5	Reasonable	Low	Low
Tape casting	Suspension	1	Good	High	Medium
Injection	Plastic material	3	Good	Medium	High

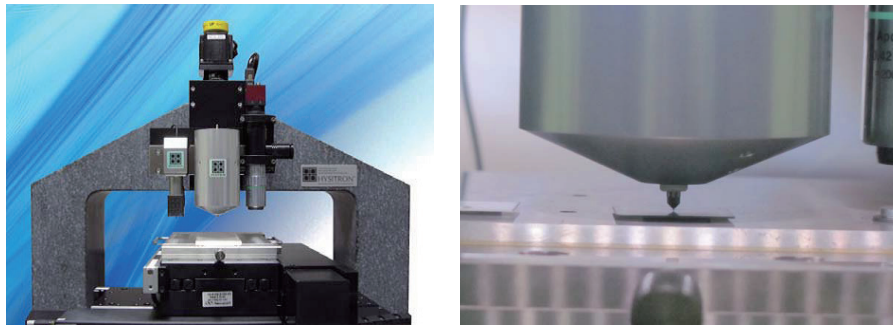

Fig. 4. (Color online) Nanoindenter bedstand.

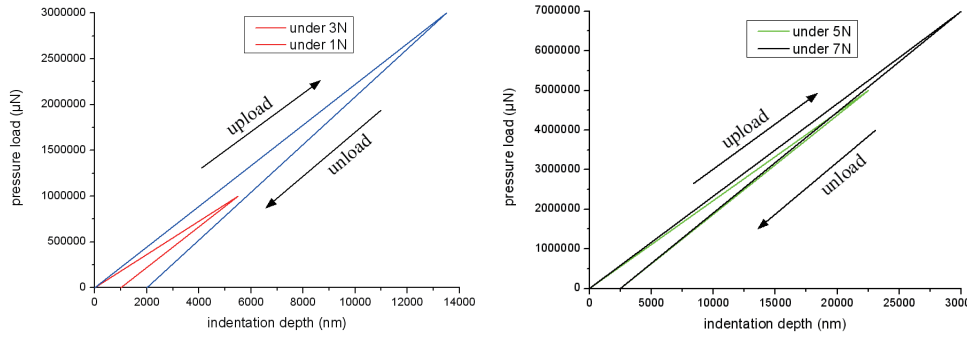

Fig. 5. (Color online) Characteristics of zirconia ceramic tape.

Table 2
Zirconia ceramic molding method.

Quantity properties	
Stabilizing agent	Y_2O_3
Unfired thickness	125 μm
X shrinkage	17.3±1%
Y shrinkage	18.3±1%

inductance coil width to spacing. The sensor resonant frequency can be calculated from the expression

$$f = \frac{1}{2\pi\sqrt{LC}}, \tag{2}$$

where L and C are inductance and capacitance, respectively. Variation of capacitance results in a change in the resonant frequency, and the change in capacitance is caused by applied pressure. A governing equation for the signal resonant frequency f as a function of pressure can be given as

$$f(P) = \frac{1}{2\pi\sqrt{L\dfrac{C_0 \tanh^{-1}\left(\sqrt{\dfrac{0.00126\cdot(D_1+D_2)\cdot P\cdot a^4}{(t_g+\frac{t_{ml}}{\varepsilon_r})\cdot D_1\cdot D_2}}\right)}{\sqrt{\dfrac{0.00126\cdot(D_1+D_2)\cdot P\cdot a^4}{(t_g+\frac{t_{ml}}{\varepsilon_r})\cdot D_1\cdot D_2}}}}}, \tag{3}$$

where C_0 is capacitance under 0 pressure, P denotes the applied pressure , a is length of a side of cavity, t_g is the cavity thickness, and ε_r is relative permittivity. $D_{1,2}$ is given by

$$D_{1,2} = \frac{Et_{m1,2}^3}{12(1-v^2)}, \tag{4}$$

where E is Young's modulus, $t_{m1,2}$ are upper and lower membrane thicknesses, respectively, and v is Poisson's ratio.

The cross section of the sensor is shown in Fig. 6. The upper and lower capacitor plates are located on the top surfaces of the fourth and first layers, respectively, and the upper capacitor plates and inductor coil are connected in series. The other end of the inductor coils achieves interconnection with the lower capacitor plate through the via to form the LC resonant circuit in Fig. 6. The geometrical parameters for the inductor and capacitor design are summarized in Tables 3 and 4, respectively.

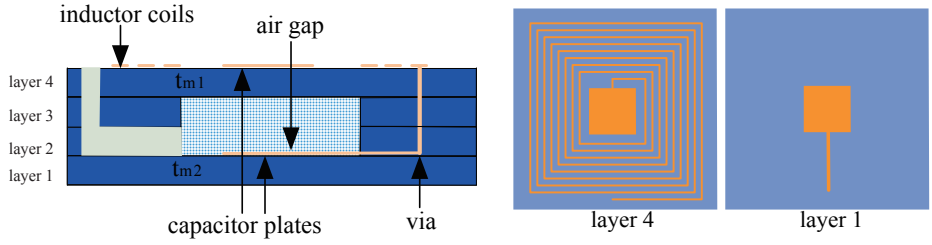

Fig. 6. (Color online) Cross section of sensor.

Table 3
Geometrical parameters of inductor design.

Symbol	Quantity	Value
din	Inner diameter of inductor coil	13.6 mm
lw	Width of inductor coil	300 μm
ls	Spacing between adjacent segments	300 μm
n	Number of inductor coils	8

Table 4
Geometrical parameters of capacitor design.

Symbol	Quantity	Value
a	Length of a side of cavity	8 mm
a_e	Length of a side of electrode	7.8 mm
t_g	Cavity thickness	250 μm

After stacking, three green tapes were sintered together, and a hollow square was cut within the second and third layers of the middle section to provide deformation space for the pressure-sensitive films. To improve the device sensitivity, the upper and lower pressure-sensitive thin films were designed in a single layer to maximize flexibility and allow for greater elastic deformation under pressure. To avoid microdevice failure, the pressure of the cavity is isolated from that of the atmosphere by sealing.

Data were obtained using the wireless measurement technique shown as a schematic electrical model in Fig. 7.[12,13] To take measurements, the reader antenna sends an alternating electromagnetic signal to the sensor inductance coils. If the signal frequency is equal to the sensor resonance frequency, the input impedance of the antenna clearly changes,[14] allowing for the determination of the sensor resonant frequency by measuring antenna impedance characteristics such as phase with an impedance analyzer.

3.2 *Fabrication*

The fabrication of an HTCC-based sensor is similar to that of an LTCC sensor and includes milling, tape casting, cutting, punching, screen printing, stacking, lamination, and firing.[15] Part of the HTCC fabrication process is shown in Fig. 8.

In fabricating the HTCC sensor, vias and cavities were drilled and then filled using screen printing. Then, the printed tapes were placed in a furnace for 20 min at 100 °C, after which layers 1, 2, and 3 were stacked and placed on a film made from carbon particles and organic solvent to form the cavity.[16,17] Finally, layer 4 was stacked onto layer 3.

Following vacuum packaging, the green tapes were isostatically laminated at a pressure of 15 MPa and a temperature of 75 °C for 20 min. Figure 9 shows the change in the constituents of the zirconia ceramic green tape, which could be joined together because the organic material became plastic after isostatic lamination and the ceramic granules on adjacent green tapes were forced together by lamination pressure. During sintering in a cofired furnace at a peak temperature of 1512 °C, the organic constituents of the tapes diffused into the air. Sintering curves for the zirconia green tape are shown

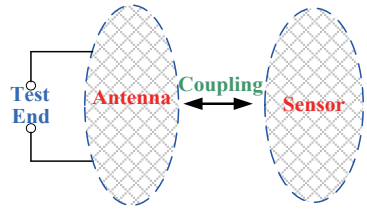

Fig. 7. (Color online) Model of sensor-antenna system.

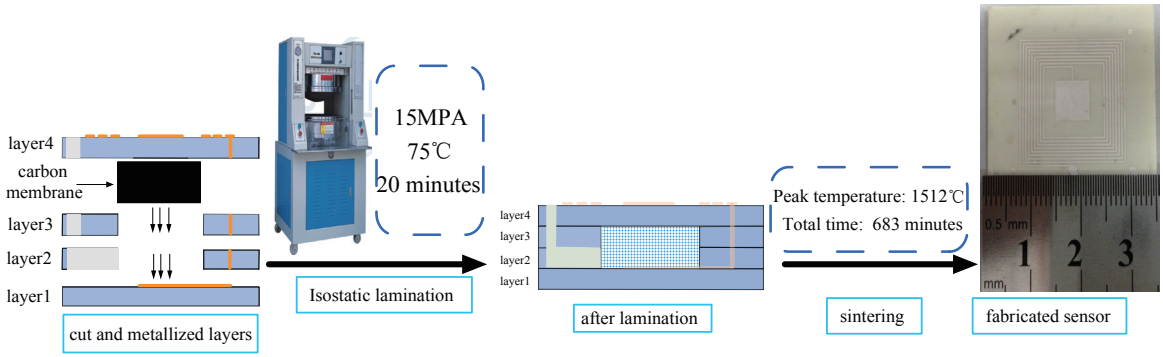

Fig. 8. (Color online) Part of fabrication process: Cut, metallize and stack. Then place a carbon membrane in the cavity. Finally, the sensor is fabricated after lamination and sintering.

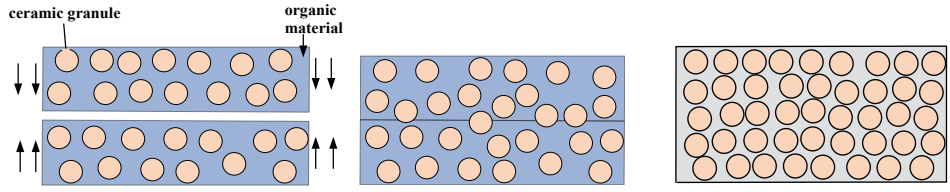

Fig. 9. (Color online) Green tape: (a) before lamination, (b) after lamination, and (c) after sintering.

in Fig. 10 and scanning electron microscopy (SEM) analyses of the cavity and sensor surfaces are shown in Figs. 11 and 12, respectively. As can be seen from Fig. 11, the cavity is well-preserved.

The sensor was sealed using a process in which a glass bead was placed on the exit hole, which was then placed in a sintering furnace. After heating at 830 °C, the glass bead covered the exit hole and effectively isolated it from the surroundings. An SEM analysis of the exit hole seal using a glass bead is shown in Fig. 13.

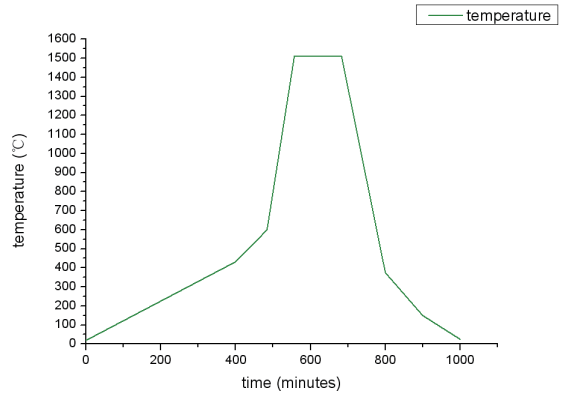

Fig. 10. (Color online) Sintering curve of zirconia green tape.

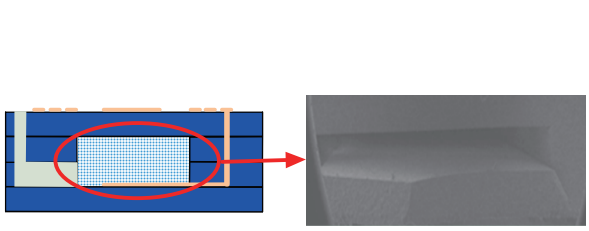

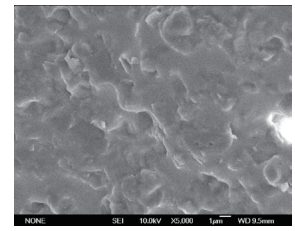

Fig. 11 (left). (Color online) SEM analysis of cavity.
Fig. 12 (right). SEM analysis of sensor surface.

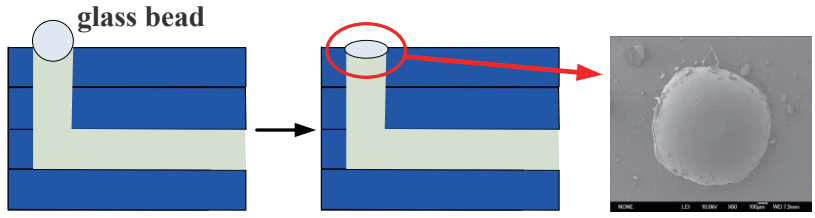

Fig. 13. (Color online) SEM analysis of exit hole sealing.

4. Results and Discussion

4.1 *Room-temperature measurement*

The frequency-pressure characteristics of the sensor at room temperature were obtained by using a measurement system that consisted of an Agilent E4991A impedance analyzer, a steel jar, a pressure control device, and a nitrogen pressure tank, as shown in Fig. 14. The measured sensor characteristics are shown in Fig. 15. As can be observed,

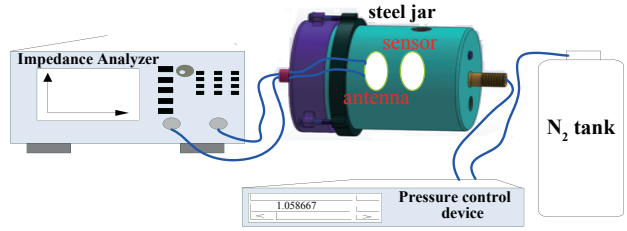

Fig. 14. (Color online) Frequency-pressure measurement system.

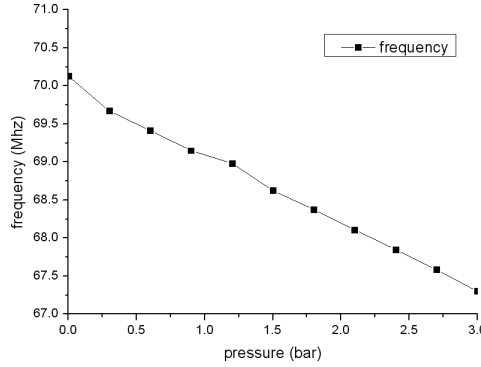

Fig. 15. Measured resonant frequency versus pressure characteristic.

the sensor resonant frequency decreases linearly with pressure, and the resonant frequency at zero pressure is 70.12 MHz, which is larger than the calculated value because the metal figure and green tape shrink after sintering. The sensitivity of the sensor is about 940 kHz/bar.

4.2 *High-temperature measurement*

The sensor characteristics as a function of temperature were then measured from room temperature to 800 °C and then at 800 °C for 30 min using a high-temperature measurement system consisting of a muffle furnace and an impedance analyzer. Owing to its higher stability under thermal stress, a tungsten wire was used to measure high temperatures. The antenna and sensor were placed in the muffle furnace, and the impedance analyzer is in a room-temperature environment. The test results in Fig. 16 proved that the sensor can be successfully coupled with a tungsten antenna at 800 °C, and they also clearly showed a reduction in frequency as the temperature increases. The average slope is −4.133 kHz/°C between 30 and 800 °C. This is mainly caused by the increase in permittivity of the sensor material, which results in an increase in capacitance. In another aspect, inductance, which increases slightly at elevated temperature, has little influence on the frequency at elevated temperature. As the sensor resonant frequency

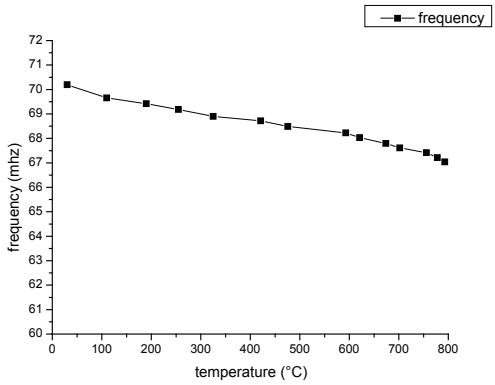

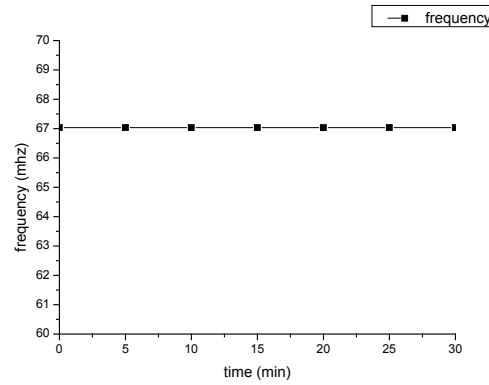

Fig. 16 (left). Sensor resonant frequency versus temperature.
Fig. 17 (right). Sensor resonant frequency at 800 °C for 30 min.

was invariant for 30 min at 800 °C shown in Fig. 17, it was clear that the sensor displayed improved stability, relative to room temperature, under these conditions.

5. Conclusions

In this paper, a resonant pressure sensor fabricated from zirconia using standard HTCC technology was shown to function equivalently to a passive LC circuit. Owing to the excellent resilience and stability of zirconia at high temperatures, the proposed sensor can be used in an environment with high thermal stress. The sensor detected pressure variations by using changes in its resonant frequency. Experimental results showed that the data can be detected at 800 °C and that the sensor has higher stability at this temperature. Owing to an almost linear response of its resonant frequency with temperature, the sensor exhibited a great deal of sensitivity to temperature change.

Acknowledgements

This work was supported by the National Basic Research Program (973) of China (No. 2010CB334703), Program for the Outstanding Innovative Teams of Higher Learning Institutions of Shanxi, Research Project Supported by Shanxi Scholarship Council of China (2013-077), and the National Natural Science Foundation of China (No. 51075375).

References

1 W. Cullinane and R. Strange: SPIE Conference on Harsh Environment Sensors. **9** (1999) 3952.

2 G. W. Hunter, R. S. Okojie, P. G. Neudeck, G. M. Beheim, G. E. Ponchak, J. Wrbanek, M. Kraskowski, D. Spry and L. Y. Chen: High Temperature Electronics, Communications, and Supporting Technologies for Venus Mission, available, http://www.mrc.uidaho.edu/~atkinson/IPPW/IPPW-5/Papers/S7_7hunter.pdf.
3 W. A. Vitriol and J. I. Steinberg: Int. J. Hybrid Microelectron. **6** (1983) 593.
4 M. A. Fonseca, J. M. English, M. Arx and M. G. Allen: J. Microelectromech. Syst. **11** (2002) 337.
5 J. English and M. G. Allen: Proc. IEEE Int. MEMS '99 12th IEEE Int. Conf. on Micro Electro Mechanical Systems, Orlando, 1999.
6 M. A. Fonseca: M A. Polymer/ceramic wireless MEMS pressure sensors for harsh environments: High temperature and biomedical applications, Georgia Institute of Technology, 2007.
7 E. D. Birdsell, J. Park and M. G. Allen: Proc. 40th AIAA Joint Propulsion Conf., Fort Lauderdale, 2004.
8 G. W. Hunter, P. G. Neudeck and R. S. Okojie: J. Turbomach. **125** (2003) 658.
9 F. Bechtold: A Comprehensive Overview on Today′s Ceramic Substrate Technologies (EMPC 2009, Rimini, 2009).
10 J. Estibaliz and A. Pajaresw: J. Am. Ceram. Soc. **90** (2007) 149.
11 K. Holmberg: Handbook of Applied Surface and Colloid Chemistry, ed. K. Holmberg (Wiley, Chichester, 2002) Chap. 1.
12 J. C. Butler, A. J. Vigliotti and F. W. Verdi: Sens. Actuators, A **102** (2002) 61.
13 R. Nopper, R. Has and L. Reindl: Instrum. Meas. **60** (2011) 2976.
14 R. Nopper, R. Niekrawietz and L. Reindl: Proc. IEEE Trans. Instrum. Meas. **59** (2010) 2450.
15 T. Thelemann, H. Thust and M. Hintz: Microelectron. Int. **19** (2002) 19.
16 H. Birol, T. Maeder and P. Ryser: Sens. Actuators, A **130/131** (2006) 560.
17 L. E. Khoong, Y. M. Tan and Y. C. Lam: J. Eur. Ceram. Soc. **30** (2010) 1973.